nature physics

Article

https://doi.org/10.1038/s41567-023-02213-1

Memory-induced Magnus effect

Received: 16 February 2023

Accepted: 16 August 2023

Published online: 21 September 2023

Check for updates

Xin Cao[1,3], Debankur Das[2], Niklas Windbacher[1], Félix Ginot[1], Matthias Krüger[2] & Clemens Bechinger[1]

Spinning objects moving through air or a liquid experience a lift force—a phenomenon known as the Magnus effect. This effect is commonly exploited in ball sports but also is of considerable importance for applications in the aviation industry. Whereas Magnus forces are strong for large objects, they are weak at small scales and eventually vanish for overdamped micrometre-sized particles in simple liquids. Here we demonstrate a roughly one-million-fold enhanced Magnus force of spinning colloids in viscoelastic fluids. Such fluids are characterized by a time-delayed response to external perturbations, which causes a deformation of the fluidic network around the moving particle. When the particle also spins, the deformation field becomes misaligned relative to the particle's moving direction, leading to a force perpendicular to the direction of travel and the spinning axis. Our uncovering of strongly enhanced memory-induced Magnus forces at microscales opens up applications for particle sorting and steering, and the creation and visualization of anomalous flows.

When a spinning object travels through a fluid, its trajectory is typically curved. Although Isaac Newton was the first to describe it in 1671 (ref. 1), this effect is commonly named after Heinrich Gustav Magnus, who provided a physical explanation on the influence of rotation on the motion of objects[2]. Nowadays, the Magnus effect is well established and is not only used in ball games but also exploited, for example, as an economic propulsion mechanism for ships[3–6] and to provide lifting forces for air vehicles[7]. In addition to such applications, Magnus effects are also relevant for understanding planet formation in protoplanetary disks[8] and the behaviour of ions in superfluids[9,10] and are even discussed in the context of the motion of vortex lines in superconductors[11,12]. In general, the Magnus force results from an asymmetry of the velocity field in the medium around a translating and simultaneously rotating object. According to the Bernoulli equation, this results in pressure inhomogeneities near the object and a force perpendicular to the direction of travel: that is, the Magnus force $\mathbf{F}_M = f(\boldsymbol{\omega} \times \mathbf{v})$, an expression that is also expected to be valid for viscous liquids at small Reynolds numbers[13]. Here the Magnus coefficient f quantifies the coupling of the particle to its surroundings, and $\boldsymbol{\omega}$ and $\mathbf{v}$ are the angular and linear velocities of the object relative to the fluid, respectively. Although in most cases $f > 0$, it can be also negative: for example, at high velocities, when the flow around the object is partially turbulent[7,14], or when spinning objects move through rarefied gases or granular media[15–17]. Whereas Magnus forces can be very strong for large objects, they are weak at small scales. In the case of Brownian particles—that is, micrometre-sized particles in simple fluids—Magnus forces eventually vanish, because viscous forces dominate over inertial effects[18,19]. Therefore, applications of Magnus forces in such systems are rare.

Here we report the experimental observation of a strong memory-induced Magnus effect for spinning micrometre-sized colloidal particles moving through an overdamped viscoelastic fluid. Unlike viscous—that is, Newtonian—liquids, which instantaneously respond to external perturbations, viscoelastic fluids are characterized by stress-relaxation times τ on the order of seconds or more[20,21]. Similar to the Magnus force $\mathbf{F}_M$ generated in a viscous liquid, in viscoelastic liquid the memory-induced Magnus force $\mathbf{F}_{mM} = \tilde{f}(\boldsymbol{\omega} \times \mathbf{v})$ is exerted on a translating and spinning object. The coefficient $\tilde{f} < 0$, and its amplitude is larger than f (that is, the coefficient in a pure viscous fluid) by a factor of more than 10^6. Our experimental results are in excellent agreement with a theoretical description in which the time-delayed response of the fluid around a moving object is modelled by a density dipole. Although this dipole points in the direction of $\mathbf{v}$ for a pure translational particle motion, it is rotated when the particle also exhibits a spinning motion. As a result, a force component perpendicular to the driving force arises, which eventually leads to $\mathbf{F}_{mM}$. This model also

[1]Fachbereich Physik, Universität Konstanz, Konstanz, Germany. [2]Institut für Theoretische Physik, Universität Göttingen, Göttingen, Germany. [3]Present address: School of Physics and Astronomy, Shanghai Jiao Tong University, Shanghai, China. e-mail: clemens.bechinger@uni-konstanz.de

https://doi.org/10.1038/s41567-023-02213-1

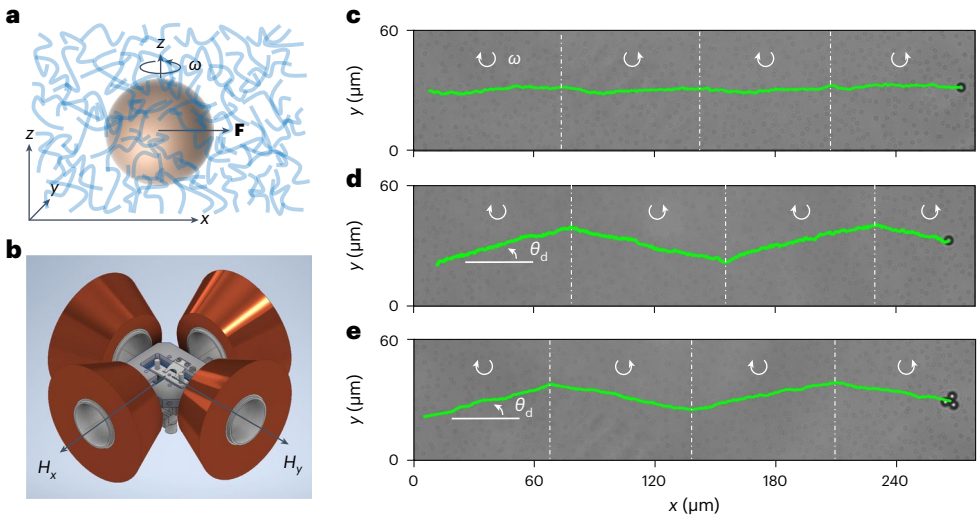

Fig. 1 | Memory-induced Magnus force acting on colloidal particles in viscous and viscoelastic fluids. a, Illustration of a superparamagnetic colloid sphere spinning at angular frequency ω (rotation axis in z direction) and driven by a force $\mathbf{F}$ along x direction through a viscoelastic fluid. **b**, Sketch of the experimental setup, with two perpendicular pairs of magnetic coils generating a rotating magnetic field $\mathbf{H}(t)$ with frequency ω_H, in the xy plane. Due to a magnetic torque the colloid is set into a spinning motion with $\omega \ll \omega_H$. **c**,**d**, Trajectories (green) of spinning colloidal particles driven through a fluid with $H = 732$ A m^{-1}, $\omega_H = 20\pi$ s^{-1} and $F = 156$ fN. The sign of the spinning direction is periodically reversed, as indicated by the curved arrows. **c**, Single colloidal particle in a purely viscous water-glycerol (1:1 by weight) mixture, for a colloid driving velocity $v_x = 0.288$ μm s^{-1}. **d**, Single colloidal particle in a 5 mM micellar solution with $v_x = 0.065$ μm s^{-1} and $\theta_d \approx 15.0^\circ$. **e**, Colloidal trimer in the same micellar solution with $v_x = 0.178$ μm s^{-1} and $\theta_d \approx 14.4^\circ$.

explains our experimental finding that when the particle's spinning motion is stopped, the force $\mathbf{F}_{mM}$ remains and only decays after time τ. Because our findings should apply to many viscoelastic fluids, we expect that this unusual type of Magnus force will lead to new applications—for example, in the field of particle sorting and steering—as well as the creation and visualization of anomalous flows[22–26].

In our experiments, we use superparamagnetic colloidal spheres (diameter $\sigma = 4.45$ μm) suspended in a viscoelastic fluid (see below) and contained in a thin sample cell. Owing to gravity, the particles sediment towards the bottom surface of the cell, where they remain during our experiments. We note, however, that trajectories similar to those that will be discussed have also been recorded for particles far from any surface (Supplementary Information). The colloid motion is imaged with a video camera mounted to an inverted microscope. After each experiment, the data are analysed using digital video microscopy. The microscope is mounted on a tilting stage, which allows an external (gravitational) drift force $\mathbf{F} = mg \sin\alpha\, \hat{\mathbf{x}}$ to be exerted on each particle. Here $mg = 286$ fN is the buoyant particle weight (obtained by multiplying the buoyant mass m and the acceleration of gravity g), α the tilting angle and $\hat{\mathbf{x}}$ the unit vector along the x direction. The angle α can be tuned between 0° and 35°, which leads to a maximum driving force of about 160 fN for a single particle or 480 fN for a colloidal trimer (see below). Additionally, we use two perpendicular pairs of coils (Fig. 1a,b) that create a rotating magnetic field $\mathbf{H}(t)$ in the sample plane, with components $H_x(t) = H\cos\omega_H t$ and $H_y(t) = H\sin\omega_H t$. The frequency $\omega_H = 20\pi$ s^{-1} is fixed in our experiments. The rotating $\mathbf{H}$ induces a rotating magnetization $\mathbf{M}$ in the colloidal particles. Owing to a phase lag in $\mathbf{M}$, the rotating magnetic field applies a torque $\Gamma = |\mathbf{M} \times \mathbf{H}| \propto H^2$ to the colloid spheres. This results in a spinning motion with angular frequency $\omega \propto \Gamma$ (see Methods and Supplementary Fig. 1 for details).

Two different types of viscoelastic fluids were used in our experiments: (1) a solution of entangled giant wormlike micelles[27] composed of about 5 mM equimolar cetylpyridinium chloride monohydrate (CPyCl) and sodium salicylate (NaSal) dissolved in water, and (2) a semidilute aqueous polymer solution of polyacrylamide (PAAM) with molecular weight 18 MDa and mass concentration 0.03%. All our experiments have been performed at a constant sample temperature of 25 °C, at which both fluids exhibit pronounced viscoelastic behaviours as confirmed by microrheological experiments[28,29] (see Methods and Supplementary Fig. 2 for details).

To demonstrate that conventional Magnus forces in colloidal systems are vanishingly small when suspended in merely viscous—that is, Newtonian—fluids[18,19], we first studied the motion of a colloidal particle in a water-glycerol mixture. Figure 1c shows the corresponding trajectory of a particle subjected to a rotating magnetic field ($H = 732$ A m^{-1}) and a driving force $F = 156$ fN. The rotation direction of $\mathbf{H}$ is periodically reversed from clockwise to anticlockwise to rule out the possible influence of particle drift in the y direction. In our experimental resolution, no particle deflection from the direction of the driving force is observed. This is consistent with the theoretically predicted conventional Magnus force in viscous liquids in the limit of low Reynolds numbers, $\mathbf{F}_M = \pi\rho(\sigma/2)^3\boldsymbol{\omega} \times \mathbf{v}$, where ρ is the fluid mass density[13,19]. For our liquid, this yields a deflection angle $\theta_d = \arctan(F_M/F) \ll 0.0002°$ (considering $\omega \ll \omega_H$), which is below the experimental resolution. When repeating the experiment in a viscoelastic fluid, however, a pronounced deflection of the trajectory is observed (Fig. 1d). From the measured velocity ratio $|v_y/v_x|$, we determine the deviation angle $\theta_d = \arctan(|v_y/v_x|) \approx 15°$. The deflection changes its direction when we reverse the direction of rotation of $\mathbf{H}$. Although we are particularly interested in the angular motion of the spinning particles, it cannot be resolved for the case of single colloidal spheres. Therefore, in the following, we use colloidal trimers whose angular motion is easily measured and that show almost identical behaviour (Fig. 1e and Supplementary Videos 1 and 2). For details about the formation of such trimers, we refer readers to the Methods section. For trimers with a spinning frequency $\omega = 0.97$ rad s^{-1} and drift velocity $v_x = 0.16$ μm s^{-1}, we find an angular deflection $\theta_d \approx 14.4°$, which demonstrates a force pointing in the direction $-\boldsymbol{\omega} \times \mathbf{v}$.

To quantify our observations, we measured the velocity ratio $|v_y/v_x|$ as a function of the trimer spinning velocity ω and for different driving forces $\mathbf{F}$ (Fig. 2a). At small ω, we observe for both viscoelastic fluids a linear behaviour that eventually saturates for larger ω (Fig. 2a, inset). In addition, $|v_y/v_x|$ is independent of v_x when ω is kept constant (Fig. 2b). Both findings indicate that in the linear regime, a memory-induced

https://doi.org/10.1038/s41567-023-02213-1

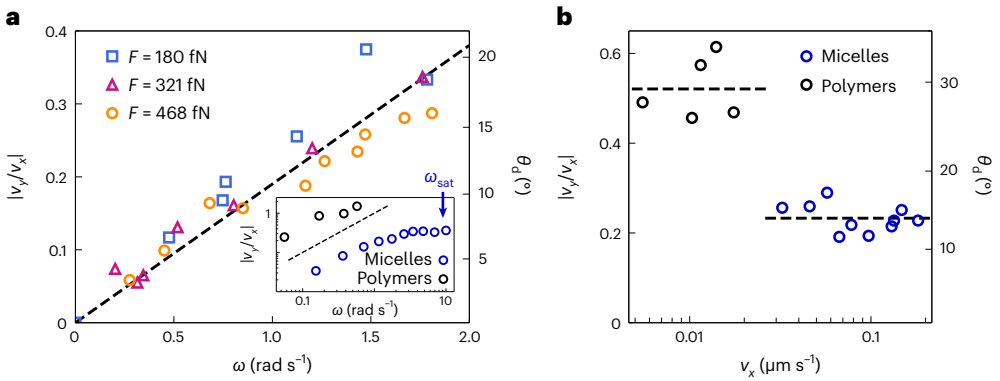

Fig. 2 | Dependence of translational and angular velocities. a, Measured velocity ratio $|v_y/v_x|$ (left axis) and deflection angle $|\theta_d|$ (right axis) of a colloidal trimer in a micellar fluid as a function of its rotational speed ω for an applied force $F = 468$ fN in x direction (orange circles), 321 fN (purple triangles) and 180 fN (blue squares), respectively. The dashed line is a fit to all data with equation $|v_y/v_x| = k\omega$ and the fitting parameter $k = 0.201 \pm 0.008$ s. Inset: $|v_y/v_x|$ as a function of ω for a colloidal trimer driving through viscoelastic PAAM (black circles) and micellar solutions (blue circles). The dashed line indicates a linear relation between $|v_y/v_x|$ and ω. The vertical arrow indicates, for micellar solution, the theoretically predicted angular frequency where $|v_y/v_x|$ saturates. **b**, $|v_y/v_x|$ and $|\theta_d|$ versus the drift velocity v_x for colloidal trimer in PAAM (black circles) and micellar solutions (blue circles). The data in PAAM and micellar solutions were obtained at magnetic fields $H = 976$ A m^{-1} and $H = 732$ A m^{-1}, respectively, which correspond to a rotational trimer velocity of $\omega \approx 0.17$ rad s^{-1} and $\omega \approx 1.2$ rad s^{-1}. Dashed lines indicate $|v_y/v_x| = 0.52$ and $|v_y/v_x| = 0.23$. The scatter in **a** and **b** is due to the measurements being performed with different colloidal trimers whose properties (magnetization, size, surface properties) vary slightly.

Magnus force $\mathbf{F}_{mM} = \tilde{f}(\boldsymbol{\omega} \times \mathbf{v})$ is acting on the colloidal trimer, with prefactor $\tilde{f}$ depending on the colloid–fluid interaction.

For a theoretical understanding of the above observations, we first consider a non-spinning particle moving at velocity $\mathbf{v}$ due to an external force $\mathbf{F}$ through a viscoelastic fluid. Owing to the finite stress-relaxation time τ, a front-back inhomogeneity in the fluid builds up around the particle. It can be characterized by a density dipole $\mathbf{p}_\parallel$ pointing in the direction of $\mathbf{v}$ (Fig. 3a, top, and Supplementary Information)[20,30–33]. In linear response theory[34], the time-dependent magnitude of $\mathbf{p}_\parallel$ is given by a history integral of the force

$$p_\parallel(t) = \int_{-\infty}^{t} \chi_T(t-t')F(t')\mathrm{d}t', \qquad (1)$$

where $\chi_T(t)$ is a memory kernel that characterizes the dipole relaxation dynamics[35]. Experimentally, $\chi_T(t)$ can be determined when the driving force acting on the particle is suddenly removed. This results in a restoring force antiparallel to $\mathbf{p}_\parallel$, leading to a recoil motion opposite to the driving direction. Figure 3b (see also Supplementary Videos 3 and 4) shows such recoil for a colloidal trimer driven by a magnetic field gradient force that was turned off at $t = 0$. In agreement with previous studies, the recoil is well described by a double-exponential decay[33,36]. From these data, we immediately obtain the memory kernel $\chi_T(t)$, as shown in Fig. 3c (see details in Supplementary Information).

When the particle is also set into a spinning motion by an external torque Γ, the orientation of the density dipole in the xy plane changes by an angle θ_p (Fig. 3a, bottom) due to the particle-fluid interaction. Accordingly, one obtains a dipole $\mathbf{p} = \mathbf{p}_\parallel + \mathbf{p}_\perp$, with $\mathbf{p}_\perp$ the component perpendicular to $\mathbf{F}$. Similar to the restoring force caused by $\mathbf{p}_\parallel$, a force perpendicular to $\mathbf{F}$ is caused by $\mathbf{p}_\perp$. This perpendicular force is identified as the memory-induced Magnus force $\mathbf{F}_{mM}$, which is proportion to $-\mathbf{p}_\perp$. We consider the regime where $\mathbf{p}_\perp$ is a linear function of $\mathbf{F}$ and Γ, for which we find (see details in Supplementary Information)

$$p_\perp(t) = \int_{-\infty}^{t} \mathrm{d}t' \chi_R(t-t')\Gamma(t')p_\parallel(t'). \qquad (2)$$

Here $\chi_R(t)$ is the memory kernel associated with the relaxation of the dipole component $p_\perp$. Because in the range of our experiments we have $\Gamma \propto \omega$ and $p_\parallel \propto F \propto v_x$ (Supplementary Fig. 3), this leads to $p_\perp \propto \omega v_x$ or $\mathbf{F}_{mM} = \tilde{f}(\boldsymbol{\omega} \times \mathbf{v})$, in agreement with the observations in Fig. 2. As a side note, we mention that after the particle starts to move in the y direction under the influence of $\mathbf{F}_{mM}$, this motion creates—similar to $\mathbf{p}_\parallel$—a further density dipole that is opposite to $\mathbf{p}_\perp$ and reduces the velocity component v_y. This effect is already included in equation (2) by considering $\chi_R(t)$ for a moving particle.

According to equation (2), $p_\perp$ (and hence $\mathbf{F}_{mM}$) should not instantaneously vanish when we remove the external torque applied to the particle. This means the particle motion in the y direction decays on a timescale given by $\chi_R(t)$ that characterizes how fast $\mathbf{p}_\perp$ decays to zero. To demonstrate this, Fig. 3d shows for $t < 0$ the motion of a trimer in the y direction under the influence of a force $F = 468$ fN in the x direction and torque $\Gamma = 66.6$ pN μm. When Γ is set to zero at $t = 0$ s, the cluster's motion in the y direction decays only on a timescale of several tens of seconds. This decay can be directly compared to the corresponding prediction (solid line) of equation (2) when assuming $\chi_R(t) \propto \chi_T(t)$. Such proportionality is plausible because the susceptibilities describe relaxations of dipole fields in different directions and can thus be expected to be similar due to isotropy of the quiescent fluid.

On the basis of the dipole-rotation picture as described in Fig. 3a, we also construct a simple Maxwell-like model for the time dependence of the dipole orientation ϕ, which contains a driving term proportional to the applied torque Γ and a restoring term owing to the relaxation of $\mathbf{p}_\perp$:

$$\dot{\phi} = C\frac{\Gamma}{\gamma_R} - \frac{\phi}{\tau} \qquad (3)$$

with γ_R the steady-state rotational friction coefficient, so that $\Gamma/\gamma_R = \omega$ is the rotational velocity of the colloid and $C \leq 1$ is a constant that describes the coupling between the rotation of the colloid and that of the density dipole. In the absence of Γ, the solution of equation (3) relaxes exponentially with a timescale τ. We remark that recent experiments[37] as well as Fig. 3b demonstrate that the relaxation process of a colloidal particle in a micellar fluid is governed by two timescales. For the sake of a minimal model, however, here only a single relaxation time is considered. Under steady-state driving conditions, the value of the dipole orientation angle ϕ becomes

$$\theta_p = C\omega\tau. \qquad (4)$$

https://doi.org/10.1038/s41567-023-02213-1

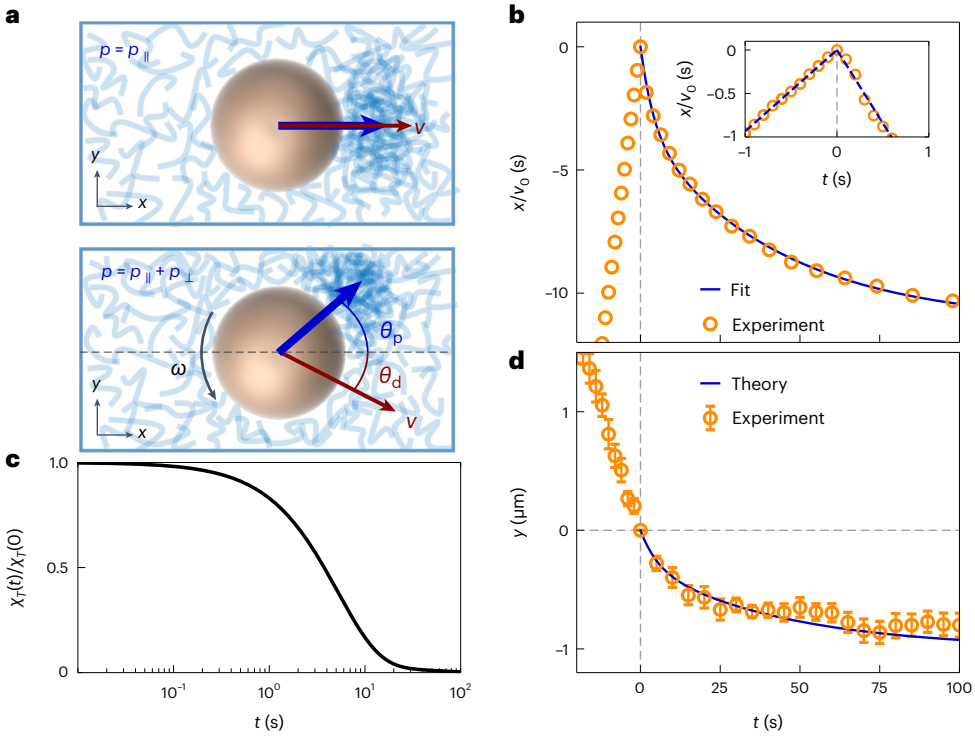

Fig. 3 | Theoretical model. a, Top, illustration of a colloidal particle moving at linear velocity **v** in a viscoelastic fluid. The linear motion deforms the microscopic network structure of the liquid, leading to a density gradient, as characterized by the density dipole $\mathbf{p}_\parallel$ parallel to **v**. Bottom, when the particle is also set into rotation ω, the dipole is rotated in the xy plane by an angle θ_p, which leads to the deflection of the particle trajectory by an angle θ_d. **b**, Measured x displacement of a non-spinning trimer (orange symbols) during a recoil experiment in which the trimer is first driven with velocity $v_0 = 0.95\ \mu m\ s^{-1}$ through the micellar fluid and the applied force is suddenly removed at t, $x = 0$. The data are normalized by v_0. The solid line represents a fitting to the equation $x = a_1 \exp(-t/\tau_1) + a_2 \exp(-t/\tau_2) - a_1 - a_2$, with $a_1 = 3.14\ \mu m$, $\tau_1 = 5.20$ s, $a_2 = 7.60\ \mu m$ and $\tau_2 = 44.5$ s. Inset: Magnified region near $t = 0$. From the ratio of the slopes (as indicated by the dashed lines) after and before $t = 0$, we obtain the recoil ratio $r = 1.8 \pm 0.1$. **c**, The memory kernel $\chi_T(t)$ (normalized by $\chi_T(0)$) as defined in equation (1), which is derived from the fitted curve shown in **b**. **d**, Measured (orange symbols) $y(t)$ displacement of a trimer in a micellar fluid that is subjected for $t < 0$ to a driving force $F = 468$ fN in the x direction and a torque $\Gamma = 66.6$ pN μm. After we set $\Gamma = 0$ at $t = 0$, the displacement in the y direction decays only after about 44.5 s. The data are averaged over 11 measurements, with the error bars corresponding to the standard deviation. The solid line is the theoretically predicted trajectory $y(t) = 0.093[a_1 \exp(-t/\tau_1) + a_2 \exp(-t/\tau_2) - a_1 - a_2]$, with a_1, τ_1, a_2 and τ_2 the same as in **b**.

Considering that the dipole force, the viscous force and the external force must balance altogether, this leads to a simple relationship between θ_p and the velocity ratio $|v_y/v_x|$ (see Supplementary Information for details):

$$\left|\frac{v_y}{v_x}\right| = r\theta_p = rC\omega\tau. \tag{5}$$

Here r is the dimensionless recoil ratio given by the ratio of the particle velocities immediately after and before turning off the driving force. From the typical recoil shown in Fig. 3b for the micellar system, we determine that $r \approx 1.8 \pm 0.1$ (a similar analysis can be applied to the PAAM solutions to obtain the corresponding r; see Supplementary Fig. 2). Equation (5) allows us to estimate $\tilde{f}$ defined above by interpreting the motion in y to arise from the force $\mathbf{F}_{mM}$. It yields $\tilde{f} = -rC\tau\gamma$, with γ the translational friction coefficient. By fitting equation (5) to the linear part of our data shown in the Fig. 2a inset, we obtain $rC\tau = 0.146 \pm 0.013$ s, or $|\tilde{f}| = 0.95 \pm 0.08\ pN\ s^2\ \mu m^{-1}$, considering $\gamma = 6.50 \pm 0.09\ pN\ s\ \mu m^{-1}$ in 5 mM micellar fluid (Supplementary Fig. 3). This is considerably larger than the Magnus coefficient for a viscous liquid, which is $f = \pi\rho(2\sigma/2)^3 = 0.28 \times 10^{-6}\ pN\ s^2\ \mu m^{-1}$ (for this estimate, we have approximated the cluster of three colloids, each with diameter σ, with a single spherical particle with diameter 2σ). We have also performed similar experiments in micellar solutions at a lower micellar concentration (4 mM), where the fluid is only slightly viscoelastic. As expected, at such low concentrations, the Magnus coefficient becomes considerably smaller (still much larger than in viscous liquid) compared to that in 5 mM due to weak colloid–fluid interaction (Supplementary Fig. 4).

In the above framework, we also obtain a simple estimate for the upper limit of ω where the linear relation between $|v_y/v_x|$ and ω ends. Assuming that the magnitude of $\mathbf{p}_\perp$ cannot exceed that of the original dipole, this yields $|v_y/v_x| < r$ (Supplementary Information). From this, one obtains a rough estimate of the saturation velocity, $\omega_{sat} \leq 1/C\tau \approx 12\ s^{-1}$, which is consistent with our data in the inset of Fig. 2a. Following a similar procedure, for a colloidal trimer in a polymer fluid, we obtain a saturation velocity of about $\omega_{sat} \leq 1/C\tau \approx 3.4\ s^{-1}$.

As an alternative approach to Magnus forces, one can introduce a viscosity tensor η_{mM}, which is defined by $\mathbf{F}_{mM} = \tilde{f}(\boldsymbol{\omega} \times \mathbf{v}) = -3\pi\sigma\eta_{mM} \cdot \mathbf{v}$. Writing the cross product using the Levi-Civita symbol, $F_{mM,i} = -\tilde{f}\omega e_{3ij}v_j$, shows that η_{mM} is anti-symmetric. When also considering the translational friction force $-\gamma\mathbf{v}$ to obtain the diagonal components of the viscosity tensor with the friction coefficient γ for $\omega = 0$, introduced below equation (5), this yields, for ω pointing in the z direction,

$$3\pi\sigma\eta_{ij} = \begin{pmatrix} \gamma & \tilde{f}\omega \\ -\tilde{f}\omega & \gamma \end{pmatrix}. \tag{6}$$

Such non-symmetric viscosity tensors (typically referred to as odd viscosity[22–26,38,39]), which generally result from the violation of Onsager's

reciprocal relations[40,41], are caused in our system by the time-delayed dynamics of the density dipole. Accordingly, the off-diagonal elements of the viscosity tensor can easily be tuned by means of the rotation frequency.

In summary, our work demonstrates that Magnus forces, which typically vanish in the realm of small Reynolds numbers, can be surprisingly strong in the case of viscoelastic fluids owing to their time-delayed response to perturbations. In addition to rotating magnetic fields, which have been used in our study to induce a spinning motion, electrical[42] and optical fields[43] have also been shown to impose considerable torques on particles down to the nanometre scale. This allows the use of Magnus forces to be extended to the regime of small Reynold numbers, which may lead to new types of microswimmers and strategies for steering and sorting particles as well as visualizing complex flow patterns in liquids. Finally, we remark that our observations bear some phenomenological resemblance to elastic turbulence. Unlike turbulence in Newtonian liquids, which only arises at high Reynolds numbers, turbulent flow patterns in viscoelastic fluids have already been observed for $\mathrm{Re} \approx 10^{-3}$ (ref. 44).

Online content

Any methods, additional references, Nature Portfolio reporting summaries, source data, extended data, supplementary information, acknowledgements, peer review information; details of author contributions and competing interests; and statements of data and code availability are available at https://doi.org/10.1038/s41567-023-02213-1.

References

1. Newton, I. A new theory about light and colors. *Am. J. Phys.* **61**, 108–112 (1993).
2. Magnus, G. Ueber die abweichung der geschosse, und: ueber eine auffallende erscheinung bei rotirenden körpern. *Ann. Phys.* **164**, 1–29 (1853).
3. De Marco, A., Mancini, S., Pensa, C., Calise, G. & De Luca, F. Flettner rotor concept for marine applications: a systematic study. *Int. J. Rotating Mach.* **2016**, 3458750 (2016).
4. Bordogna, G. et al. Experiments on a Flettner rotor at critical and supercritical Reynolds numbers. *J. Wind Eng. Ind. Aerodyn.* **188**, 19–29 (2019).
5. Bordogna, G. et al. The effects of the aerodynamic interaction on the performance of two Flettner rotors. *J. Wind Eng. Ind. Aerodyn.* **196**, 104024 (2020).
6. Seddiek, I. S. & Ammar, N. R. Harnessing wind energy on merchant ships: case study Flettner rotors onboard bulk carriers. *Environ. Sci. Pollut. Res.* **28**, 32695–32707 (2021).
7. Seifert, J. A review of the Magnus effect in aeronautics. *Prog. Aerosp. Sci.* **55**, 17–45 (2012).
8. Forbes, J. C. Curveballs in protoplanetary discs—the effect of the Magnus force on planet formation. *Mon. Not. R. Astron. Soc.* **453**, 1779–1792 (2015).
9. Donnelly, R. J. & Roberts, P. Stochastic theory of the interaction of ions and quantized vortices in helium II. *Proc. R. Soc. Lond. A. Math. Phys. Sci.* **312**, 519–551 (1969).
10. Sonin, E. Magnus force in superfluids and superconductors. *Phys. Rev. B* **55**, 485 (1997).
11. Ao, P. & Thouless, D. J. Berry's phase and the Magnus force for a vortex line in a superconductor. *Phys. Rev. Lett.* **70**, 2158 (1993).
12. Yao, Y., Tang, Y. & Ao, P. Generating transverse response explicitly from harmonic oscillators. *Phys. Rev. B* **96**, 134414 (2017).
13. Rubinow, S. I. & Keller, J. B. The transverse force on a spinning sphere moving in a viscous fluid. *J. Fluid Mech.* **11**, 447–459 (1961).
14. Kim, J., Choi, H., Park, H. & Yoo, J. Y. Inverse Magnus effect on a rotating sphere: when and why. *J. Fluid Mech.* **754**, R2 (2014).
15. Borg, K. I., Söderholm, L. H. & Essén, H. Force on a spinning sphere moving in a rarefied gas. *Phys. Fluids* **15**, 736–741 (2003).
16. Kumar, S., Dhiman, M. & Reddy, K. A. Magnus effect in granular media. *Phys. Rev. E* **99**, 012902 (2019).
17. Seguin, A. Forces on an intruder combining translation and rotation in granular media. *Phys. Rev. Fluids* **7**, 034302 (2022).
18. Changfu, Y., Haiying, Q. & Xuchang, X. Lift force on rotating sphere at low Reynolds numbers and high rotational speeds. *Acta Mech. Sin.* **19**, 300–307 (2003).
19. Solsona, M. et al. Trajectory deflection of spinning magnetic microparticles: the Magnus effect at the microscale. *J. Appl. Phys.* **127**, 194702 (2020).
20. Dhont, J. K. *An Introduction to Dynamics of Colloids* Ch. 5 (Elsevier, 1996).
21. Larson, R. G. *The Structure and Rheology of Complex Fluids* Ch. 3 (Oxford Univ. Press, 1999).
22. Banerjee, D., Souslov, A., Abanov, A. G. & Vitelli, V. Odd viscosity in chiral active fluids. *Nat. Commun.* **8**, 1573 (2017).
23. Souslov, A., Dasbiswas, K., Fruchart, M., Vaikuntanathan, S. & Vitelli, V. Topological waves in fluids with odd viscosity. *Phys. Rev. Lett.* **122**, 128001 (2019).
24. Yang, Q. et al. Topologically protected transport of cargo in a chiral active fluid aided by odd-viscosity-enhanced depletion interactions. *Phys. Rev. Lett.* **126**, 198001 (2021).
25. Kalz, E. et al. Collisions enhance self-diffusion in odd-diffusive systems. *Phys. Rev. Lett.* **129**, 090601 (2022).
26. Reichhardt, C. & Reichhardt, C. Active rheology in odd-viscosity systems. *Europhys. Lett.* **137**, 66004 (2022).
27. Cates, M. & Candau, S. Statics and dynamics of worm-like surfactant micelles. *J. Phys. Condens. Matter* **2**, 6869 (1990).
28. Narinder, N., Bechinger, C. & Gomez-Solano, J. R. Memory-induced transition from a persistent random walk to circular motion for achiral microswimmers. *Phys. Rev. Lett.* **121**, 078003 (2018).
29. Ginot, F. et al. Recoil experiments determine the eigenmodes of viscoelastic fluids. *New J. Phys.* **24**, 123013 (2022).
30. Dzubiella, J., Löwen, H. & Likos, C. Depletion forces in nonequilibrium. *Phys. Rev. Lett.* **91**, 248301 (2003).
31. Squires, T. M. & Brady, J. F. A simple paradigm for active and nonlinear microrheology. *Phys. Fluids* **17**, 073101 (2005).
32. Rauscher, M., Domínguez, A., Krüger, M. & Penna, F. A dynamic density functional theory for particles in a flowing solvent. *J. Chem. Phys.* **127**, 244906 (2007).
33. Khan, M., Regan, K. & Robertson-Anderson, R. M. Optical tweezers microrheology maps the dynamics of strain-induced local inhomogeneities in entangled polymers. *Phys. Rev. Lett.* **123**, 038001 (2019).
34. Chaikin, P. M. & Lubensky, T. C. *Principles of Condensed Matter Physics* Ch. 7 (Cambridge Univ. Press, 1995).
35. Kubo, R. Statistical-mechanical theory of irreversible processes. I. General theory and simple applications to magnetic and conduction problems. *J. Phys. Soc. Jpn.* **12**, 570–586 (1957).
36. Gomez-Solano, J. R. & Bechinger, C. Transient dynamics of a colloidal particle driven through a viscoelastic fluid. *New J. Phys.* **17**, 103032 (2015).
37. Caspers, J. et al. How are mobility and friction related in viscoelastic fluids? *J. Chem. Phys.* **158**, 024901 (2023).
38. Markovich, T. & Lubensky, T. C. Odd viscosity in active matter: microscopic origin and 3D effects. *Phys. Rev. Lett.* **127**, 048001 (2021).
39. Lou, X. et al. Odd viscosity-induced Hall-like transport of an active chiral fluid. *Proc. Natl Acad. Sci.* **119**, 2201279119 (2022).
40. Onsager, L. Reciprocal relations in irreversible processes. I. *Phys. Rev.* **37**, 405 (1931).
41. Onsager, L. Reciprocal relations in irreversible processes. II. *Phys. Rev.* **38**, 2265 (1931).

42. Fennimore, A. et al. Rotational actuators based on carbon nanotubes. *Nature* **424**, 408–410 (2003).
43. Kuhn, S. et al. Optically driven ultra-stable nanomechanical rotor. *Nat. Commun.* **8**, 1670 (2017).
44. Groisman, A. & Steinberg, V. Elastic turbulence in a polymer solution flow. *Nature* **405**, 53–55 (2000).

Methods

Sample preparation

We prepare highly diluted colloidal suspensions of superparamagnetic spheres (Dynabeads M-450, diameter ~4.5 μm) dispersed in a viscoelastic fluid. The number density (roughly 10^8 per litre) corresponds to fewer than ten colloid spheres in our field of view, $240 \times 300\ \mu m^2$. For viscoelastic fluid, we use either a polymer solution or a micellar solution. The polymer solution is a semidilute aqueous solution of PAAM with molecular weight 18 MDa and mass concentration 0.03%. The micellar solution is an equimolar, aqueous solution of CPyCl and NaSal. The molar density is 5.5 mM for the data in Fig. 2a and 5.0 mM for the Fig. 2a inset and all other relevant data. To make a colloid sample, we inject the colloid suspension into a glass sample cell about $20 \times 10 \times 0.2\ mm^3$ in size, where 0.2 mm is the sample thickness. After the sample is made, it is transferred to an inverted Nikon microscope where we can observe the motion of the colloid. During the experiment, the temperature of the sample is kept at $25 \pm 1\ ^\circ C$ using a flow thermostat.

Formation of colloidal trimers

The rotating magnetic field creates an effective long-range attraction ($\propto r^3$) between the magnetic colloids[45]. In the presence of a rotating magnetic field with $H = 732\ A\ m^{-1}$, colloidal particles with distances of ~5σ experience a strong attraction and form dense clusters (Supplementary Video 5). To increase the chance of particle encounters during the cluster formation process, the sample stage is tilted by ~10°. This leads to the formation of rigid and stable colloidal clusters with random sizes, including trimers.

Calibration of magnetic torques

Due to the large viscosity in our experiments, the rotating speed of the colloids is much less than the rotating frequency 10 Hz of the magnetic field. This leads to a time-averaged magnetic torque of $\Gamma = \gamma_m H^2$ (ref. 46) applied by the rotating magnetic field, as shown in Fig. 1b. In steady rotation, the magnetic torque balances the viscous torque of the fluid: that is, $\Gamma = \gamma_R \omega$, where $\gamma_R = 6\pi\eta\sigma^3$ for colloid trimers[47]. This leads to $\omega = kH^2$, where $k = \gamma_m/\gamma_R$. To calibrate the magnetic torque, we first rotate the colloid trimer in water, where the measured rotating speed ω of a colloid trimer as a function of H exactly follows the equation $\omega = kH^2$, as shown in Supplementary Fig. 1, with the fitted $k = 3.26 \times 10^{-5}\ m^2\ A^{-2}\ s^{-1}$. Considering the measured $\eta = 1.29 \times 10^{-3}$ Pa s for water and the colloid diameter $\sigma = 4.45\ \mu m\ s^{-1}$, we obtain $\gamma_m = 6.99 \times 10^{-5}\ pN\ \mu m\ A^{-2}\ m^2$.

Colloidal recoils with time-dependent magnetic gradients

Because gravitational drift forces on the particles cannot be suddenly changed, the translational recoil curves shown in Fig. 3b are measured using a permanent magnet whose position in the sample plane can be suddenly changed (<0.1 s) with a mechanical spring-loaded device. To do so, we first put the magnet close to the sample cell, where the magnetic field gradient leads to a constant drift velocity for the trimers. When we activate the spring-loaded retraction mechanism, the magnet is pulled away and the colloidal recoil sets in.

Data availability

Source data are provided with this paper. All relevant data are also available from the corresponding author on reasonable request.

References

45. Martinez-Pedrero, F. & Tierno, P. Magnetic propulsion of self-assembled colloidal carpets: efficient cargo transport via a conveyor-belt effect. *Phys. Rev. Appl.* **3**, 051003 (2015).
46. Janssen, X., Schellekens, A., Van Ommering, K., Van Ijzendoorn, L. & Prins, M. Controlled torque on superparamagnetic beads for functional biosensors. *Biosens. Bioelectron.* **24**, 1937–1941 (2009).
47. Cao, X. et al. Moiré-pattern evolution couples rotational and translational friction at crystalline interfaces. *Phys. Rev. X* **12**, 021059 (2022).

Acknowledgements

We acknowledge helpful discussions with M. Fuchs, P. Tierno, G. Junot and A. Ping. This work is funded by the Deutsche Forschungsgemeinschaft (DFG), grant no. SFB 1432 – Project ID 4252172. F.G. acknowledges support from the Humboldt foundation.

Author contributions

C.B. and X.C. designed the experiments, which were carried out and analysed by X.C. and N.W. The theoretical model was developed by D.D. and M.K. F.G. contributed to overall discussions. All authors contributed to the writing of the paper.

Competing interests

The authors declare no competing interests.

Additional information

Supplementary information The online version contains supplementary material available at https://doi.org/10.1038/s41567-023-02213-1.

Correspondence and requests for materials should be addressed to Clemens Bechinger.

Peer review information *Nature Physics* thanks Jure Dobnikar and the other, anonymous, reviewer(s) for their contribution to the peer review of this work.